ICES Journal of Marine Science, 2025, Vol. 82, Issue 9, fsaf160
https://doi.org/10.1093/icesjms/fsaf160
Received: 7 April 2025; **revised:** 19 August 2025; **accepted:** 21 August 2025
Original Article

Broadband and narrowband echosounder signals produce comparable estimates of volume backscattering

Robert M. Levine [1,*], **Christopher Bassett** [2], **Alex De Robertis** [1]

[1]Resource Assessment and Conservation Engineering Division, Alaska Fisheries Science Center, National Marine Fisheries Service, National Oceanic and Atmospheric Administration, Seattle, WA 98115, United States
[2]Applied Physics Laboratory, University of Washington, Seattle, WA 98105, United States

*Corresponding author. Resource Assessment and Conservation Engineering Division, Alaska Fisheries Science Center, National Marine Fisheries Service, National Oceanic and Atmospheric Administration, 7600 Sand Point Way NE, Seattle, WA 98115, United States. E-mail: Robert.Levine@noaa.gov

Abstract

Despite the potential benefits for species identification, broadband acoustic data collection has yet to be widely implemented in fisheries surveys. In large parts, this is because it remains unclear whether broadband echo integration produces similar abundance estimates as traditional narrowband data. This work compares the integration of broadband and narrowband data from EK80 transceivers operating at nominal frequencies of 38, 70, 120, and 200 kHz. We sequentially transmitted broadband frequency modulated (FM) and narrowband continuous wave (CW) pings to investigate the relationship between the volume backscattering coefficients measured using the two signal types, $S_{V,CW}$ and $S_{V,FM}$. $S_{V,FM}$ was calculated using two approaches. The first approach calculated the pulse-compressed volume backscatter in the time domain, $S_V(t)$, using three different methods for estimating aggregate terms in place of frequency-dependent terms. The second approach calculated the mean volume backscatter in the frequency domain, $S_V(f)$. While time-domain estimates provide reasonable first approximations of $S_{V,FM}$, calculation of volume backscatter using the mean of $S_V(f)$ produces backscatter estimates that are statistically equivalent to those calculated from $S_{V,CW}$. These comparisons indicate that broadband signals processed in the frequency domain can be echo integrated for fisheries surveys, maintaining continuity of long-term indices of abundance and biomass.

Keywords: acoustic survey; echo integration; EK80; broadband; fisheries acoustics

Introduction

Broadband echosounders offer the potential for improved classification of acoustic targets via increased spectral content relative to the narrowband echosounders currently used in most fisheries acoustics surveys (Lavery et al. 2007, Bassett et al. 2018). However, broadband signals have yet to be widely adopted in fisheries surveys in part due to uncertainty whether echo integration of broadband signals is equivalent to that produced with the conventional narrowband signals used in long-standing time series. These surveys depend on the application of consistent methodology to ensure that estimates of fish abundance by species and size derived from echo integration of volume backscattering (Simmonds and MacLennan 2005) are comparable over time. Measurements showing that new acoustic instrumentation or processing techniques provide comparable, or better, echo integration are needed to transition to new methodology for scientific and management applications. For this reason, previous transitions to new acoustic instrumentation have merited investigation (Jech et al. 2005, Macaulay et al. 2018, De Robertis et al. 2019).

Over the past decade, advances in commercial echosounders have led to more widespread application of echosounder systems capable of broadband operation into platforms including fisheries survey and oceanographic vessels (Demer et al. 2017), cabled infrastructure (Ona et al. 2020), moorings (Levine et al. 2024b), and uncrewed vehicles (Benoit-Bird and Waluk 2020, Bassett et al. 2022, Grassian et al. 2023). A notable example of this is the development of the widely used Kongsberg Simrad EK80 echosounder, which can transmit and process both continuous wave (CW, hereafter also referred to as narrowband) signals as well as linear frequency modulated (FM, hereafter also referred to as broadband) signals (Demer et al. 2017).

Broadband signals offer several potential benefits over narrowband signals. The range resolution of the pulse compressed signal is proportional to the inverse of the transmitted frequency bandwidth rather than the pulse duration (Chu and Stanton 1998, Ehrenberg and Torkelson 2000), which can improve resolving individual scatterers (Lavery et al. 2017). Theory suggests that signal-to-noise ratios (SNR) are also improved by pulse compression techniques (Chu and Stanton 1998, Ehrenberg and Torkelson 2000). Perhaps most compelling among the benefits is the potential to improve taxonomic classification via frequency-based estimation of scatter composition (Lavery et al. 2007, 2010, Bassett et al. 2018, Blanluet et al. 2019, Benoit-Bird and Waluk 2020, Cotter et al. 2021, Urmy et al. 2024), and remote estimation of scatterer size and orientation (Stanton et al. 2012, Loranger et al. 2022, Kubilius et al. 2023, Tuser et al. 2023, Pedersen et al. 2024).

In contrast to narrowband signals, which are processed in the time domain using well-established methods and calibration coefficients (Demer et al. 2015), processing of broadband signals is more complex and requires more decisions from the user (Lavery et al. 2017). Broadband signals can be processed in either the time or frequency domain. Generally, time domain signals are processed using the matched filter, or pulse compression, method (Turin 1960, Chu and Stanton 1998). The details of this approach are critical as they provide the

Published by Oxford University Press on behalf of International Council for the Exploration of the Sea 2025. This work is written by (a) US Government employee(s) and is in the public domain in the US.

Downloaded from https://academic.oup.com/icesjms/article/82/9/fsaf160/8262704 by National Marine Mammal Lab user on 26 September 2025

Table 1. Method and calibration parameters used for the six echo integration datasets.

Method	Approach	Gain selection	α	Ψ
G_{CW}	Time domain (CW)	G_{CW}	α_{CW}	Ψ_{CW}
G_{fc}	Time domain (FM)	$G(f_c)$	$\alpha(f_c)$	$\Psi(f_c)$
$\bar{G}_f$	Time domain (FM)	Mean over f	Mean over f	Mean over f
G_{int}	Time domain (FM)	Sphere integration	Mean over f	Mean over f
$\overline{S_V(f)}$	Freq. domain (FM)	$G(f)$	$\alpha(f)$	$\Psi(f)$
$\overline{S_V(f_{CW})}$	Freq. domain (FM)	$G(f)$	$\alpha(f)$	$\Psi(f)$

There are four methods using the time-domain approach: narrowband processing (G_{CW}), use of gain at the center frequency (G_{fc}), average across the bandwidth ($\bar{G}_f$), and gain derived from the integration of the calibration sphere (G_{int}). For the frequency-domain methods, $\overline{S_V(f_{CW})}$ represents the integration in the frequency domain over a bandwidth consistent with narrowband measurements, and $\overline{S_V(f)}$ represents integration based on the full band. The absorption coefficient (α) and two-way equivalent beam angle (Ψ) used are shown for each approach.

theoretical a basis for establishing equivalence between echo integration of signals regardless of whether they are narrowband or broadband. In the time domain, pulse compression employs cross-correlation, or convolution, of a replica signal with scattered signals. When the frequency content of a signal is of interest, pulse compressed signals are typically transformed to the frequency domain using a discrete Fourier transform. Critically, a discrete Fourier transform is a linear operation. Thus, the energy in the temporal domain is equal to that in the frequency domain (Rudin 1987). Theory therefore suggests that time- and frequency-domain processing techniques should produce equivalent echo integration results if processed correctly.

Despite the potential advantages of broadband signals for echo classification and the theoretical expectation of equivalent echo integration performance, adoption of these methods in abundance surveys has been slow and many applications of fisheries echosounders continue to rely on narrowband data. To take advantage of the improved capabilities offered by use of broadband signals in this context, it must be demonstrated that echo integration of broadband signals does not increase the uncertainty or introduce bias in abundance estimates. The primary approach to echo integration of broadband data has been to use time-domain processing (Andersen et al. 2024) where the calibration parameters are not explicitly frequency dependent. Rather, calibration parameters such as gain, equivalent beam angle, and absorption coefficients are calculated at a single frequency. For example, gain has been computed at the center (Blanluet et al. 2019, Loranger et al. 2022) or nominal (Jech et al. 2017) frequency of the transmit signal in different studies. This approach is likely to be a simplification, summarizing complex calibration parameters in a single value (Bodholt 2002, Andersen et al. 2024), and as such has primarily been employed for the purpose of displaying calibrated pulse compressed data. Alternatively, one could calculate volume backscatter in the frequency domain, including all frequency-dependent calibration parameters, and subsequently average across a portion or the entirety of the bandwidth.

There has yet to be a standardized and well-validated procedure for echo integration of broadband data, which presents a barrier to confidently introducing broadband observations into existing time series of acoustic-derived abundance estimates made with traditional narrowband instruments. The goal of this paper is to compare different approaches for processing broadband signals to investigate whether broadband transmit pulses can be echo integrated to obtain equivalent values to their narrowband counterparts. If this is the case, it will open the door to operate echosounders in broadband mode without sacrificing the quality of critical quantitative echo integration measurements needed to meet survey requirements and other scientific objectives.

Methods

We investigated two potential approaches encompassing five methods for echo integration of broadband data and compared the results with a single standard method for narrowband integration (Table 1). These methods were selected as they are the most commonly employed in frequency- and time-domain processing of acoustic data. The first approach calculates the pulse-compressed volume backscatter in the time domain, $S_V(t)$ (dB re 1 m^{-1}; MacLennan et al. 2002), using aggregate calibration terms in place of frequency-dependent terms (see Supplementary Material A1; Andersen et al. 2024). Calculation in the time domain assumes uniform sensitivity across frequency, as it applies single-frequency or band-averaged terms such as gain and two-way equivalent beam angle (e.g. gain computed at the center frequency of the bandwidth; Lavery et al. 2017, Andersen et al. 2024).

The second approach we explored is the use of volume backscatter in the frequency domain, $S_V(f)$, which, given its applications for echo classification, is a typical product of interest for broadband data. This approach requires more complex processing as it applies frequency-dependent quantities to compute volume backscatter (Supplementary Material A1; Andersen et al. 2024). However, this likely better accounts for the frequency dependence of the calibration, changes in sampling volume, transmission loss, and transmit/receive sensitivity of the signal. The resulting $S_V(f)$ is then averaged over the full ($\overline{S_V(f)}$) and narrower CW-equivalent ($\overline{S_V(f_{CW})}$) bandwidth, combining contributions from all frequencies within those bands to calculate a single estimate of volume backscatter.

This paper assumes a familiarity with the fundamental characteristics of narrowband and broadband signals used in echosounding applications and associated terminology (MacLennan et al. 2002). Readers unfamiliar with these principles should refer to references including Ehrenberg and Torkelson (2000), Stanton and Chu (2008), Stanton et al. (2012), and Demer et al. (2017) for more information.

Data collection

Data were collected during acoustic-trawl surveys in the Gulf of Alaska (10–17 March 2022) and the Eastern Bering Sea (4 June to 5 August 2022) on the NOAA ship *Oscar Dyson* (Fig. S1). Walleye pollock (*Gadus chalcogrammus*) dominates

Downloaded from https://academic.oup.com/icesjms/article/82/9/fsaf160/8262704 by National Marine Mammal Lab user on 26 September 2025

Table 2. Transmit parameters used for each transducer.

Transducer	ES38-7	ES70-7C	ES120-7C	ES200-7C
Nominal frequency (f_{nom}, kHz)	38	70	120	200
FM centre frequency (f_c, kHz)	39.5	70	125	212.5
FM transmit range (kHz)	34–45	50–90	95–155	165–260
Pulse duration (ms)	1.024	1.024	1.024	1.024
Transmit power (W)	2000	750	250	105

CW transmissions were at the nominal frequency. The same pulse duration and transmit power were used for the CW and FM signals.

the biomass in acoustic-trawl surveys in both regions (De Robertis et al. 2021, Levine and Jones 2025). Measurements were made with split-beam Kongsberg EK80 echosounders operating at 38 (ES38-7), 70 (ES70-7C), 120 (ES120-7C), and 200 kHz (ES200-7C). The transducers were mounted on the ship's centreboard at a depth of 9.15 m. Data presented here were collected opportunistically between survey transects at ship speeds of $\sim$ 0–2.5 m s^{-1} in bottom depths of $\sim$ 30–1300 m. A total of 39 collection events (Fig. S1), averaging 3.8 h of data collection per event, were completed. Collections were conducted in relatively high and consistent fish density, and at slow speeds to minimize inter-ping variability given the relatively slow ping rate used in the study (described below).

The echosounders were configured to alternate between narrowband and broadband transmissions using the 'Advanced Sequencing' option in the EK80 software (Simrad 2022). While the CW signals were transmitted simultaneously, the FM signals were transmitted sequentially to eliminate any potential for interference between FM channels (i.e. crosstalk; Khodabandeloo et al. 2021, 2024). The echosounder repeated a cycle of five pings: a narrowband ping transmitted at all four frequencies simultaneously followed by sequential FM pings at 38, 70, 120, and 200 kHz. All data were collected at the maximum ping rate possible such that time between successive pings was twice the time required to sample to the bottom to avoid observation of the bottom echo from the previous ping (range of 0.5–4 pings s^{-1}; Renfree and Demer 2016). The transmit parameters used are included in Table 2.

Echosounder calibration

Five calibrations were conducted between 1 January and 5 August 2022 following the standard sphere method (Demer et al. 2015), with the echosounders operated in the same configuration used during data collection. The primary output of a calibration is echo integration gain (G, equivalent to $10log_{10}[g]$ as presented in Andersen et al. [2024]), which has a large influence over echo integrals (S_V) in both time- and frequency-domain processing. For example, in logarithmic terms, S_V is proportional to $-2G$ (see Supplementary Material).

Calibrations were conducted at all frequencies using a 38.1-mm tungsten carbide sphere suspended at a range of 18–25 m. During four of the calibrations, a 22-mm tungsten carbide sphere was suspended 5 m below the 38.1-mm sphere. The same spheres and suspension mechanism were used for all calibrations, using copolymer line as suggested by Renfree et al. (2020). These concurrent observations were used to produce additional estimates of gain for the 120- and 200-kHz channels (Fig. 1) as described in the following sections. The use of two spheres reduced spectral gaps in the 120- and 200-kHz channels caused by excluding sphere responses near the nulls during calibration processing (Lavery et al. 2010). Sound speed (Chen and Millero 1977) and absorption (Francois and Garrison 1982a, b) were computed at each calibration site from a conductivity temperature and depth (Sea-Bird Scientific 911plus) cast from the average of the water column profile between the transducer face and depth of the calibration sphere.

Narrowband calibration gain

The on-axis echo integration CW gain (G_{CW}, Gain + S_A correction parameter from EK80 software) was estimated for all events (red dots, Figs 1 and 2) using the EK80 software calibration tool (Simrad 2022). For the four calibration events where the 22-mm sphere was included, the final CW gain at 120 and 200 kHz were computed as the linear average of the results from the two spheres (mean pairwise absolute difference of 0.3 and 0.8 dB at 120 and 200 kHz, respectively). This was done to match the use of both spheres for broadband calibration (see below). Assuming each calibration is valid with the potential for random error, all five calibrations were then averaged in linear units and back-transformed to compute a single gain G_{CW} at each frequency.

Broadband calibration gain

The echo integration gain as a function of frequency, $G(f)$, was estimated for all FM channels using EK80 calibration software (note that the S_A correction is always 0 for FM calibrations). Gain curves for the 38- and 70-kHz channels were determined using the 38.1-mm sphere. In broadband measurements with common sphere diameters, 120 and 200 kHz have one or more nulls in the frequency spectra making it difficult to estimate gains across the transmitted bandwidth. The gaps created by these nulls were filled by combining the calibrations from both spheres (e.g. Lavery et al. 2017). For a given frequency f where data from only one sphere was available due to the nulls, $G(f)$ was assigned the corresponding gain from that sphere. Where data were available from both spheres, the gains from both spheres were averaged in the linear domain. To address any remaining gaps and produce values at regular intervals of f (calibration results are reported in intervals of 99–856 Hz), the resulting $G(f)$ for each event were linearly interpolated at an interval of 100 Hz.

To calculate $S_V(t)$ using pulse-compressed broadband samples, a single value of gain measured at the centre frequency (f_c) of the channel bandwidth was used in place of frequency-dependent terms (Equation 30 in Andersen et al. 2024). For each channel, the gain at the centre frequency G_{fc} was selected from the estimates of $G(f)$ from each calibration event (blue, Fig. 2).

To further evaluate the influence of gain selection on the calculation of $S_V(t)$, two alternative single-value representations of gain were calculated. Using the estimates of $G(f)$ from each calibration event, the mean gain over the bandwidth of each

Downloaded from https://academic.oup.com/icesjms/article/82/9/fsaf160/8262704 by National Marine Mammal Lab user on 26 September 2025

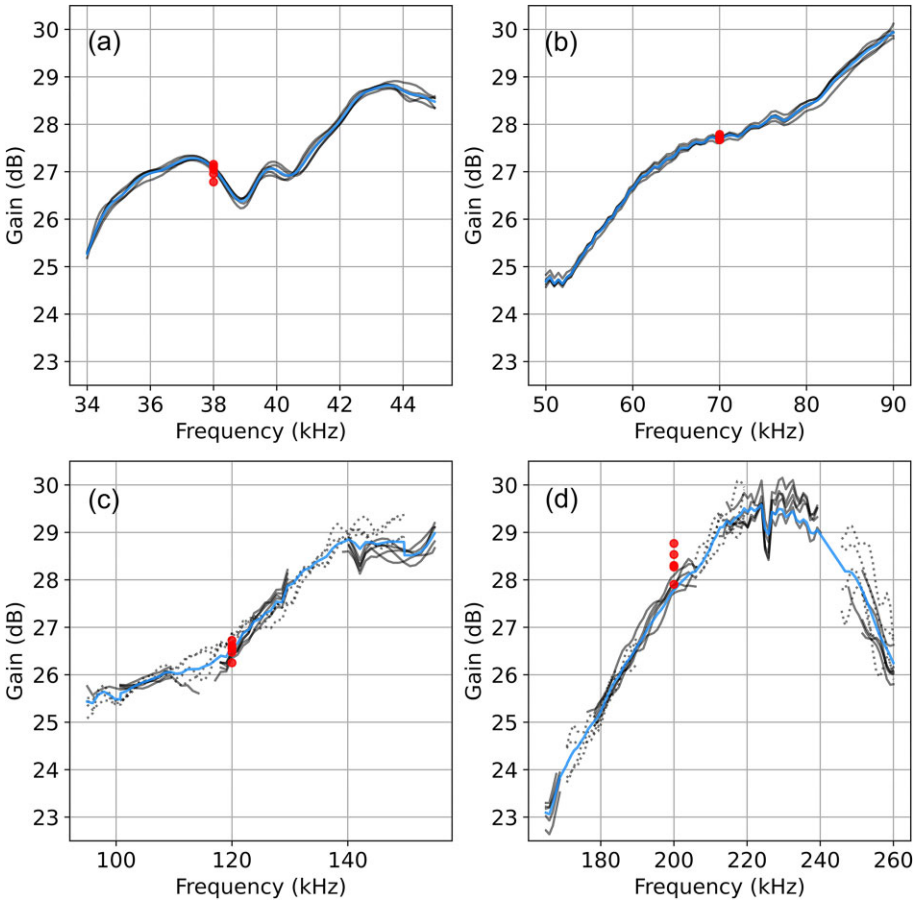

Figure 1. Gain curves for the (a) 38-, (b) 70-, (c) 120-, and (d) 200-kHz channels (nominal frequencies). The solid lines are calibrations using a 38.1-mm tungsten carbide sphere and dotted lines at 120 and 200 kHz show the calibrations using a 22-mm tungsten carbide sphere. The blue line indicates the average of the linearly interpolated gains for all calibration events. Red circles indicate calculated gain for CW signal.

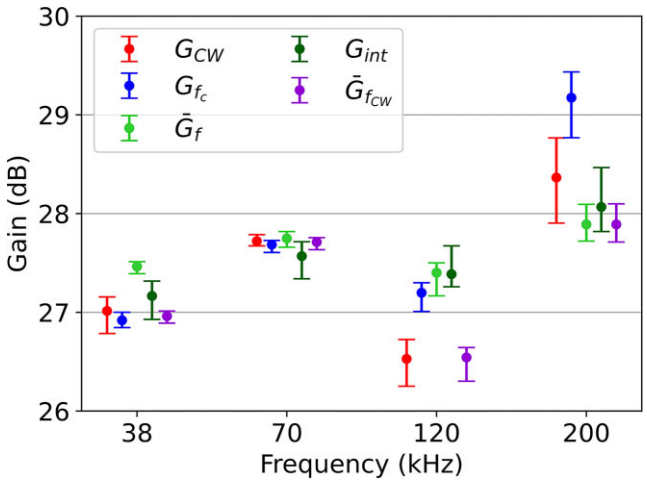

Figure 2. Calibration gains calculated for CW (G_{CW}, red) and FM pings at the centre frequency (G_{f_c}, blue), using the mean across the band ($\bar{G}_f$, light green), and using on-axis integration methods (G_{int}, green). For comparison, the mean of $G(f)$ within the bandwidth equal to the CW band ($\bar{G}_{f_{CW}}$, purple) is included. The circle indicates the mean value at each frequency and the whiskers indicate the minimum and maximum values.

channel ($\bar{G}_f$, light green, Fig. 2) was calculated as

$$\bar{G}_f = 10log_{10}(\hat{g}), \quad (1)$$

where $\hat{g}$ is the linear average of the gains reported in the calibration results for all n values of f calculated as

$$\hat{g} = n^{-1} \sum_n 10^{\left(\frac{G(f_n)}{10}\right)}. \quad (2)$$

A third estimate of gain (G_{int}) was derived via integration of the calibration sphere (dark green, Fig. 2). With allowances for the differences in FM processing, this method can be thought of as analogous to the calibration method applied in narrowband calibrations. For each channel and calibration, the target strength ($TS(t)$, dB re 1 m^2, MacLennan et al. 2002) was calculated for every sample (Andersen et al. 2024, Equation 25) using a single nominal gain value. Single targets were detected (Ona and Barange 1999) and restricted to the known range of the sphere ($\pm$ 2 m). On-axis targets were determined by restricting single targets to those with a maximum physical angle of 0.2 degrees, which corresponds to beam compensation of $<$ 0.05 dB for the 7° transducers used in this study. Pings which met those criteria were used to calculate the mean sphere range and mean observed sphere TS. $S_V(t)$ was calculated for these on-axis pings by integrating the data within $\pm$ 1.5 m of the sphere into a single value from which an observed nautical area backscattering coefficient (s_A, m^2

Downloaded from https://academic.oup.com/icesjms/article/82/9/fsaf160/8262704 by National Marine Mammal Lab user on 26 September 2025

Table 3. Gain (G) and two-way equivalent beam angle (Ψ) used for calculating $S_V(t)$ using the three broadband (G_{fc}: centre frequency, $\bar{G}_f$: mean across the band, G_{int}: on-axis integration) and CW (G_{CW}) methods, calculated as the average across all five calibrations.

	Gain					EBA		
f_{nom} (kHz)	G_{CW}	G_{fc}	$\bar{G}_f$	G_{int}	$\bar{G}_{fcw}$	Ψ	$\Psi(f_c)$	$\bar{\Psi}$
38	27.01	26.92	27.46	27.17	27.04	−20.70	−21.04	−20.95
70	27.72	27.69	27.75	27.57	27.69	−20.70	−20.70	−20.33
120	26.53	27.20	27.40	27.39	26.57	−20.70	−21.05	−20.80
200	28.37	29.17	27.89	28.07	27.89	−20.70	−21.23	−21.00

The average gain of the narrowband-equivalent portion of the bandwidth centred on the nominal frequency ($\bar{G}(f_{CW})$) is shown for reference.

nmi^{-2}; MacLennan et al. 2002), $s_{A,obs}$, was computed. The expected reference target strength (TS_{ref}), calculated using the linear average of $TS(f)$, was determined based on the sphere size, bandwidth, and environment (Demer et al. 2017). A reference s_A ($s_{A,ref}$) was calculated from TS_{ref}, range (r), the two-way equivalent beam angle (Ψ, equivalent to $10log_{10}(\psi)$ in Andersen et al. 2024), and range to the sphere (r_{target}), where

$$s_{A,ref} = \frac{10^{\frac{TS_{ref}}{10}} \times 4\pi \times 1852^2}{10^{\frac{\Psi}{10}} \times {r_{target}}^2}. \quad (3)$$

The corrected S_V gain (G_{int}) was calculated by adjusting the nominal gain used to initially calculate S_v (G_{nom}):

$$G_{int} = G_{nom} - \frac{10log_{10}\left(\frac{s_{A,ref}}{s_{A,obs}}\right)}{2}. \quad (4)$$

Given that each calibration was considered valid, variation between calibrations was assumed to represent random error. Thus to parameterize with our best estimate of calibration parameters, all five calibrations were averaged in linear units and back-transformed to compute a single gain for each method as was done for the narrowband gain.

Data processing

All data processing was conducted in Python using the pyEcholab library (Wall et al. 2018) for raw data processing and an implementation of the broadband data processing and associated Python scripts presented in Andersen et al. (2024). Narrowband data were processed according to established methods (Simmonds and MacLennan 2005). Broadband data were processed in both the time and frequency domain using each gain type and additional calibration coefficients (Table 1).

Echo integration in the time domain

Volume backscatter (S_V) was calculated in the time domain ($S_V(t)$) for narrowband data and the three variations of single-value broadband gains (Table 1). When calculating $S_V(t)$ using G_{int} and $\bar{G}_f$, the mean two-way equivalent beam angle was used, calculated as the linear average of $\Psi(f_n)$ for all n values of f (Table 1). Values of $\Psi(f_n)$ were calculated following Andersen et al. (2024) (their equation 29), as

$$\Psi(f_n) = \Psi(f_{nom}) + 20log10\left(\frac{f_{nom}}{f_n}\right) + 20log10\left(\frac{c^2}{{c_o}^2}\right), \quad (5)$$

where $\Psi(f_{nom})$ is the logarithmic two-way equivalent beam angle at the nominal frequency measured by the manufacturer in a tank. The inclusion of $20log10(c^2/{c_o}^2)$ is to correct for the effect of the local sound speed at the time of data collection (c) relative to the sound speed during the manufacturer measurement in a tank under different sound speeds (c_o) (Bodholt 2002). Since all analyses conducted here were conducted on S_V ratios that are unaffected by this term (it cancels out when computing ratios), this was left out and the original manufacturer values of $\Psi(f_n)$ were used (Table 1). Although this correction generally has a small effect, this term should be included in standard processing. The value of $\Psi(f_n)$ where $f_n = f_c$ was used for calculations using G_{fc}. The mean absorption coefficient (α, dB m^{-1}) was calculated in 100-Hz intervals across the bandwidth of the channel following Francois and Garrison (1982a, b), with the value at f_c used for G_{fc} calculations and linearly averaged for the other two gain types (Table 1). The gain and two-way equivalent beam angle values used in data processing are shown in Table 3.

Echo integration in the frequency domain

Volume backscatter spectra $S_V(f)$ were calculated on a ping-by-ping basis using 2-m data windows from 5 m below the transducer to 5 m above the sounder-detected seafloor, with the centre of a new data window taken every 0.5 m (75% overlap). The individual data windows of resulting spectra within every 50 ping (horizontal) by 5 m (range) integration cell were averaged in linear units to produce a single $S_V(f)$ per cell (Fig. 3). The spectra were then further averaged in linear units across the entirety of the channel bandwidth, $\overline{S_V(f)}$, to produce a single value of S_V for each integration cell. To investigate the impact of integrating across a limited section of the bandwidth, a second $S_V(t)$ equivalent was calculated by averaging a subset of $S_V(f)$ around the nominal frequency corresponding to the bandwidth of the equivalent narrowband signal, $\overline{S_V(f_{CW})}$. A CW-equivalent bandwidth of 976 Hz was used based on the pulse duration of 1.024 ms for all channels (Table 2), calculated as $1/\tau$, where τ is the pulse duration in seconds (Simmonds and MacLennan 2005).

Comparison of echo integrals

Volume backscatter for both narrowband and broadband signals were integrated into 50 ping (horizontal) by 5 m (range) cells from 5 m below the transducer to 5 m above the sounder-detected seafloor for comparison. The narrowband signals were processed in the same manner as in standard acoustic-trawl surveys of the area (De Robertis et al. 2021, Levine and Jones 2025). To remove cells dominated by noise, estimates of noise in each cell were calculated using passive data collection of both signal types recorded before each sampling event. When passive data were not available (15 of 39 collection events), background noise was calculated from ac-

Downloaded from https://academic.oup.com/icesjms/article/82/9/fsaf160/8262704 by National Marine Mammal Lab user on 26 September 2025

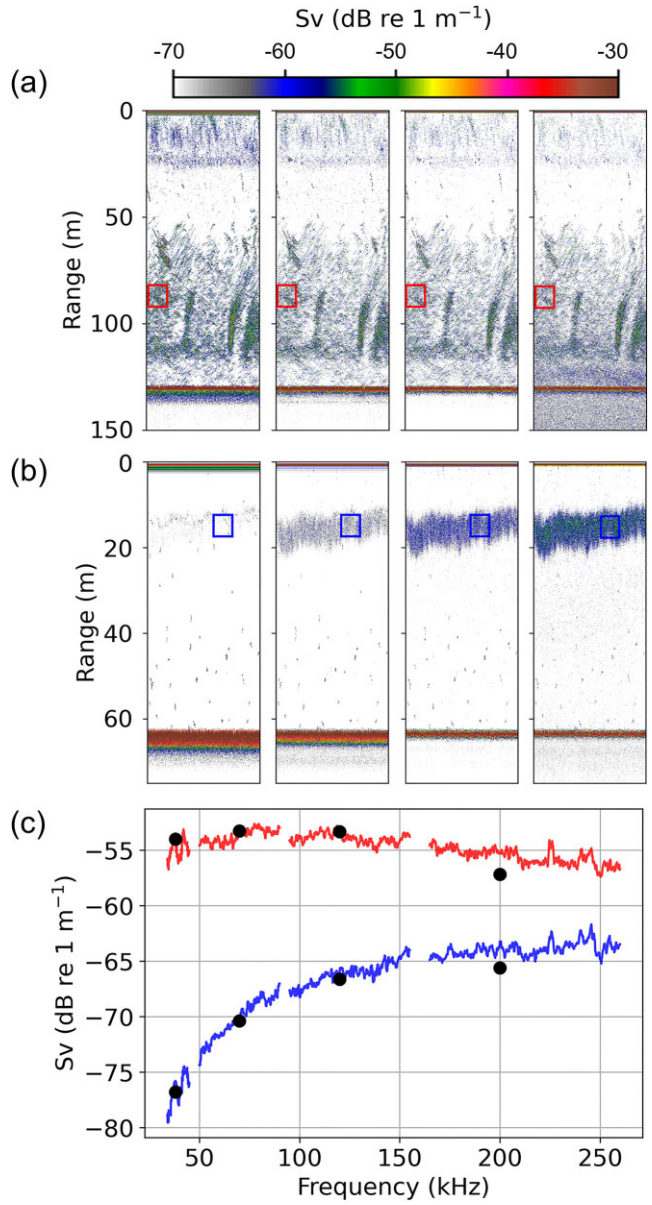

Figure 3. Example echograms at 38, 70, 120, and 200 kHz (left to right) during observations of (a) fish and (b) zooplankton. (c) Mean $S_V(f)$ of the red and blue regions indicated on the echograms. The black circles indicate the CW S_V in the corresponding regions.

tive transmissions following De Robertis and Higginbottom (2007). Methods for noise estimation are not well developed for FM signals. As a first-order approximation, we applied the methods used for CW data to the G_{fc} FM processed data. Integration cells with an SNR < 10 dB in either the CW or G_{fc} datasets were removed from subsequent analyses. Analysis was further restricted to relatively strong scatterers using a S_V integration threshold of −70 dB re 1 m^{-1}, as in acoustic-trawl surveys of these areas (Levine and Jones 2025). The nautical area backscattering coefficient s_A was calculated in each cell.

The gridded datasets were further averaged into single values integrated from 5 m below the surface to 5 m above the seafloor in 15-minute intervals. In order to assess the significance of differences between s_A of both signal types, the mean and 95% CIs of the $s_{A,FM}/s_{A,CW}$ ratio were estimated using the methods in De Robertis et al. (2019). For each calculation method, a bootstrap sample j was generated by drawing a random sample of the available 5953 15-min intervals with replacement, from which the ratio r'_j was calculated as

$$r'_j = \frac{s_{A,FM,j}}{s_{A,CW,j}}, \tag{6}$$

and the mean ratio for the bootstrap sample was computed by averaging the ratios in the logarithmic domain and back-transforming to linear units:

$$\hat{r}' = 10^{\left[n^{-1}\sum_n log_{10}(r'_j)\right]}. \tag{7}$$

Given the use of average gains when calculating s_A, the influence of calibration uncertainty (i.e. variability between calibration) was estimated by calculating a linear calibration factor g'. For each iteration, n = 5 calibration events were drawn with replacement and linear averaged (G_{boot}) for each pulse type and compared to the mean gains $\bar{G}_{FM}$ and $\bar{G}_{CW}$ used for post-processing,

$$g' = \frac{10^{\left[\frac{2\left(G_{FM,boot}-\bar{G}_{FM}\right)}{10}\right]}}{10^{\left[\frac{2\left(G_{CW,boot}-\bar{G}_{CW}\right)}{10}\right]}}. \tag{8}$$

The estimates of the FM/CW echo integration ratio were then modified by the calibration factor as

$$\hat{r}'_{tot} = \hat{r}'g'. \tag{9}$$

For each FM gain type, the mean and 95% CIs of $\hat{r}'_{tot}$ were calculated using 5000 bootstrap realizations.

To evaluate the influence of frequency response on the variability between broadband- and narrowband-derived volume backscatter, we compared cells with distinct scattering responses consistent with those of fish and zooplankton. For every cell in which data from all four narrowband frequencies had an SNR ≥ 10 dB (no integration threshold was applied during this analysis), CW S_V at all frequencies was normalized to the 38-kHz backscatter (frequency differencing, Korneliussen and Ona 2003). These cells were then clustered using the K-means algorithm (Lloyd 1982). The optimal number of clusters ($k = 5$) was determined using an elbow analysis for k = 1:10. The mean and 95% percentiles of the s_A ratios were computed from integration cells for the clusters exhibiting narrowband frequency responses consistent with those previously reported for pollock and zooplankton (krill) in this area (De Robertis et al. 2010, Bassett et al. 2018).

Results

In total, ∼ 2.3 × 10^6 pairs of pings containing broadband and narrowband observations were collected at the four frequencies during the 39 collection events. The initial gridding into 50 ping by 5 m cells resulted in 60 584 cells. Restricting grid cells to those with an SNR ≥ 10 dB for both narrowband and broadband observations further reduced the number of valid cells (ranging from 4.2% reduction at 38 kHz to 35.8% reduction at 200 kHz). The implementation of a −70 dB re m^{-1} integration threshold created the greatest reduction of the dataset, with 37.4%, 33.6%, 33.7%, and 24.9% of the original grid cells remaining after filtering at 38, 70, 120, and

Downloaded from https://academic.oup.com/icesjms/article/82/9/fsaf160/8262704 by National Marine Mammal Lab user on 26 September 2025

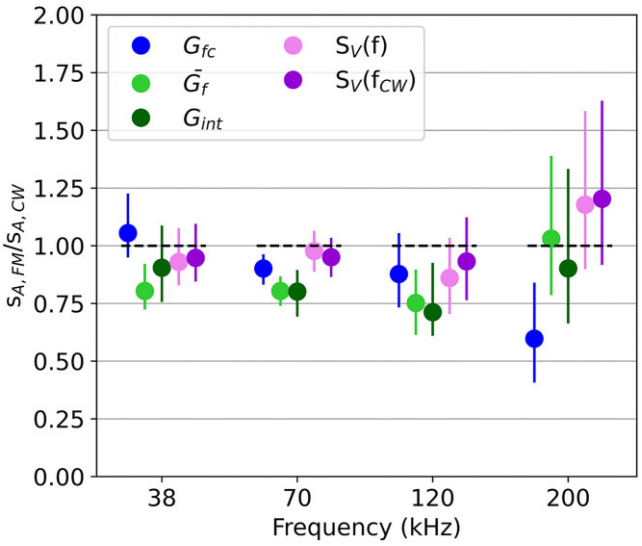

Figure 4. Mean FM/CW echo integration ratios and 95% CIs including the calibration uncertainty for all 15-minute intervals of paired FM and CW integrated water column observations using −70 dB re 1 m^{-1} integration threshold. Estimates of s_A were calculated using gains calculated at the centre frequency (G_{fc}), using the mean across the band ($\bar{G}_f$), using on-axis integration methods (G_{int}), using the average of the volume backscattering spectrum across the entire bandwidth ($S_V(f)$) and a subset of the bandwidth equal to the CW band ($S_V(f_{CW})$).

200 kHz, respectively. After further integrating the entire water column in 15-minute intervals, the final dataset contained 558–613 15-minute intervals of paired FM and CW observations depending on frequency.

The average ratio between estimates of broadband integrated backscatter ($s_{A,FM}$) and narrowband integrated backscatter ($s_{A,CW}$) varied as a function of gain selection and calculation method. For all versions of $S_V(t)$, the 95% intervals of the $s_{A,FM}/s_{A,CW}$ ratios differed from 1.0 for least two of the four frequencies (Fig. 4). Data calculated using parameters at the centre frequency, G_{fc}, resulted in significantly different ratios (i.e. confidence intervals did not overlap with 1) at both 70 and 200 kHz while $\bar{G}_f$ (applying the mean gain across the bandwidth) was significantly different at all frequencies except 200 kHz where it produced the mean ratio closest to 1. Given that the time-domain methods were calculated using the same equations, these differences are attributed to the uncertainties associated with the use of single values for frequency-dependent calibration parameters. The G_{int} integration method was statistically equivalent to CW at 38 and 200 kHz but not at 70 and 120 kHz. Given that the absolute magnitude of the error bars of the $s_{A,FM}/s_{A,CW}$ ratios (Fig. 4) are similar to those of calibration alone (Fig. S2), it appears that most of the uncertainty in these ratios is attributable to calibration.

In contrast, the $s_{A,FM}/s_{A,CW}$ ratios calculated from $\overline{S_V(f)}$ were not significantly different from 1 at any frequency (Fig. 4). Thus, $\overline{S_V(f)}$ is deemed to produce estimates of volume backscatter comparable with narrowband data. While time-domain processing produced comparable estimates for some frequencies, $\overline{S_V(f)}$ was the only method to do so across all frequencies tested. Using only the equivalent narrowband portion of the bandwidth of the FM signal, $\overline{S_V(f_{CW})}$, resulted in similar ratios as $\overline{S_V(f)}$ that were also not significantly different from 1. This suggests that integrating over a wider bandwidth around the nominal frequency does not affect the comparison to the narrowband estimate for these scatters. Ping-to-ping variability of $S_V(f)$ computed in narrow bandwidths was higher than for the full bandwidth (Fig. S3). However, $S_V(f)$ processed in CW-equivalent bandwidth was consistent with the variability observed in the CW data suggesting similar information content (Fig. S3).

The use of $\overline{S_V(f)}$ for integration also produced echo integrals consistent with narrowband methods for scatterers with distinctly different responses. K-mean clustering resulted in the selection of 5693 and 2114 cells exhibiting frequency responses consistent with pollock and krill, respectively (Fig. 5a, total $n = 38\,559$). Ratios of $s_{A,FM}/s_{A,CW}$ show minimal variability between fish and zooplankton cells, with no significant difference between narrowband and broadband integration results for either scatterer type (Fig. 5b). Due to the smaller cell size used, variability between cells resulted in large confidence intervals compared with water column integration comparison (Fig. 4). The consistency between the narrowband and broadband integration for the zooplankton-like cells (Fig. 5) indicated that $\overline{S_V(f)}$ produces equivalent echo integration to CW signals for weak targets (as the −70 dB re 1 m^{-1} integration threshold was not applied).

Discussion

This comparison indicates that frequency-dependent volume backscatter from broadband signals processed in the frequency domain can achieve comparable results to narrowband methods. In other words, $S_{V,FM}$ calculated from $\overline{S_V(f)}$ can be used to echo integrate in place of $S_{V,CW}$. Even when averaging across a smaller portion of the total bandwidth equivalent to that of the CW signal, the use of $\overline{S_V(f)}$ accounts for the frequency-dependence of the system sensitivity, which likely explains the improved performance over more simplified time-domain approximations. The equivalence between narrowband and broadband echo integrated results using $\overline{S_V(f)}$ provides an opportunity to expand the use of advanced capabilities (e.g. improved echo classification) without interfering with the core objectives of acoustic-trawl surveys (e.g. estimate abundance and continue existing time series).

The decision to use narrowband or broadband signals should ultimately be informed by the application. Currently, narrowband data is the primary data type used for echo integration in acoustic-trawl surveys. Our results suggest that if broadband data collection is desired for secondary applications (e.g. to inform taxonomic classification) the best approach for integration is to calculate and integrate volume scattering spectra. This is more computationally expensive than the direct integration of the time-domain signal, but can be overcome with improved computer hardware and software. In addition, relative to narrowband data collection, broadband data collection requires higher data volumes (in this study, the broadband data volume was 14 times larger than narrowband). In cases where only a single frequency is used for abundance estimation, or a subset of pings collected in broadband can provide the frequency resolution required for additional objectives, the mixing of narrowband and broadband collection can be considered.

Downloaded from https://academic.oup.com/icesjms/article/82/9/fsaf160/8262704 by National Marine Mammal Lab user on 26 September 2025

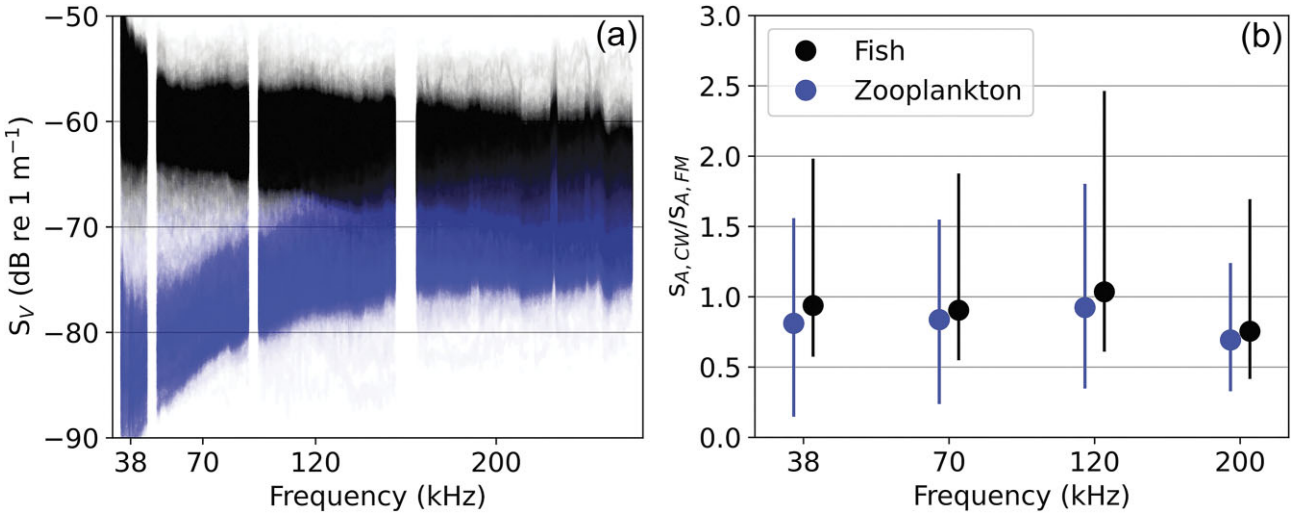

Figure 5. (a) Frequency response for a subset of 5 m by 50 ping integration cells with scattering consistent with fish ($n = 5693$, black) and zooplankton ($n = 2114$, blue). (b) Ratio of $s_{A,CW}$ and $s_{A,FM}$ for the included integration cells when calculated using $S_V(f)$. The circle indicates the mean and the lines show the 95% CIs.

In many applications, the magnitude of the uncertainties corresponding with the narrowband to broadband ratios shown in Fig. 4 may not be the largest driver of uncertainty in acoustic estimates of abundance. Uncertainties in calibration (Demer et al. 2017, Renfree et al. 2020), species identification, acoustic properties of the scatterers (Simmonds and MacLennan 2005), and behavior and size (Hazen and Horne 2004, De Robertis et al. 2019) can lead to variability in volume scattering larger than the differences in processing methods explored here. The deviation of the $s_{A,FM}/s_{A,CW}$ ratio from $r = 1$ across the methods in Fig. 4 is likely relatively small compared to the uncertainties in the final estimates of abundance of a given species when considering all of these factors. Thus, an adequate accounting for all uncertainties in a given application would, in many cases, suggest that impacts of the signal type or processing methods are not the dominant source of error. While the uncertainty associated with time-domain methods is unlikely to affect the conclusions of previous studies applying these methods, echo integration in the frequency domain should be the preferred method for quantitative echo integration going forward.

The ability to assess the difference between narrowband- and broadband-derived estimates of s_A largely relies on the accuracy and precision of the calibration. While it is possible that there are unrecognized differences between narrowband and broadband echo integration, their magnitude is smaller than that of the calibration variability and unlikely to be important in practice. Given the large volume of data averaged in this study, most of the uncertainty in the $s_{A,FM}/s_{A,CW}$ ratio is likely driven by calibration uncertainty (i.e. the magnitude of the uncertainty due to the gain alone (Fig. S2) is comparable with that of the total integration ratios). Calibration uncertainty tends to increase with frequency (De Robertis et al. 2019) which is evident as higher variability between repeated calibrations (Fig. 1). This can be driven by variability in the suspension apparatus (Renfree et al. 2020) or lower target SNR. Assuming the calibrations are accurate (i.e. on average, the gain of the system is correctly represented), the precision of the calibrations (i.e. variability between calibrations) was the primary factor affecting the confidence intervals of the echo integration ratios (Fig. 4).

Integration of broadband data in the time domain depends on single-values (Table 1) to parameterize a complex non-linear relationship. This does not adequately account for the non-linear frequency-dependence in instrument parameters (gain, two-way equivalent beam angle), physical properties (absorption), and target scattering responses. And while there are other potential ways to summarize calibration parameters not explored here (e.g. selection of parameters at f_{nom}), the unlikelihood of capturing these nonlinear calibration parameters remains. Gain, for example, varies across the total bandwidth by up to ~ 4–7 dB (Fig. 1) which results in a change of 8–14 dB in volume backscatter. Summarizing gain to a single value by sub-selecting (G_{fc}, G_{f_n}), averaging ($\bar{G}_f$), or integrating the sphere response across all frequencies (G_{int}), does not adequately represent the gain curves. For example, the effectiveness of using the commonly employed G_{fc} for broadband integration may depend on the centre of the bandwidth relative to the nominal frequency of the narrowband data being used for reference. An instance of this occurs in the 200 kHz results presented here, where G_{fc} is > 1.2 dB higher than $\bar{G}_f$. In this case, the value at the centre frequency is a poor representation of the observed gain across the bandwidth. The steep slope in gain between f_{nom} and f_c (Fig. 1) translates to a large deviation from the narrowband backscatter between these two estimates (Fig. 4). In contrast, the use of $\overline{S_V(f_{CW})}$ accounts for the frequency dependence and thus more accurately represents the behavior of the signal near f_{nom} regardless of the larger transmit bandwidth. Thus, whether integrating the entire band or sub-selecting a portion of the bandwidth, this variability can only be fully accounted for when calculating volume backscatter in the frequency domain as the first step.

We found that averaging only a small subset of the bandwidth in the frequency domain, in this case equivalent to the narrowband signal, resulted in equivalent estimates of volume backscatter between narrowband and broadband signals. While there is inherent value to using a wider bandwidth for

Downloaded from https://academic.oup.com/icesjms/article/82/9/fsaf160/8262704 by National Marine Mammal Lab user on 26 September 2025

both echo integration and species discrimination applications, processing of smaller sub-bands of the broadband signal may have benefits, such as restricting the signal bandwidth to address potential crosstalk (Khodabandeloo et al. 2024), reducing the size of the processed dataset for storage and archiving, as well as in situations where the useful portion of the band is limited due to noise or interference from other acoustic systems. Ping-to-ping variance is higher when using a subset of the bandwidth to calculate $\overline{S_V(f)}$ (Fig. S3). However, as when processing spectra (Bassett et al. 2018), this variance can be reduced by averaging more observations (i.e. larger integration cells). Thus, in practice, this increased variability is likely to have only a limited impact on echo integration results in many applications.

While increased confidence in the effectiveness of echo integration of broadband data may facilitate wider adoption for many applications, challenges remain with regards to the collection and post-processing of broadband signals that should be considered before transitioning towards new methods. Relative to narrowband signals, data volumes are larger. This larger data volume also increases the complexity of post-processing, increases processing time, and puts more requirements on the software and computers used for processing and analysis. While most common software for fisheries acoustics can be used to analyse broadband data, processing is neither standardized nor as accessible as narrowband data processing. The lack of standardized methods also applies to parameterization of processing beyond calibration, such as proper selection of the data window length and overlap (Lavery et al. 2017, Bassett et al. 2018, Liu et al. 2023), and requires thoughtful consideration specific to the application. Future work should include the development of and consensus on useful guidelines for the selection and implementation of these processing parameters, with considerations for acoustic-trawl surveys as well as other applications.

While broadband pulse compression is expected to improve signal-to-noise (Chu and Stanton 1998, Ehrenberg and Torkelson 2000), in practice this benefit may not be realized. Using the same 1.024 ms pulse duration for both signal types, background noise was consistently higher in the broadband data than the narrowband data (Table S1, Fig. S4). This increased sensitivity to noise was apparent at all frequencies, though was substantially higher ($\geq$10 dB) at 70 kHz and above. This background noise was range limiting, particularly at 200 kHz where background noise was on average 16 dB higher in the FM data than CW. The increased noise at equivalent pulse durations could be due to a larger bandwidth and thus higher susceptibility to electrical, ambient, and/or noise spikes from the vessel (Mitson 1995), with electrical noise dominating at higher frequencies and propulsion noise at lower frequencies in many cases (e.g. De Robertis and Higginbottom 2007). When using the same pulse duration, relative to the narrowband data, one might expect shorter observation ranges for broadband data, particularly at higher frequencies. Depending on the application, broadband signals can be configured and/or processed to reduce noise. Broadband signals can be collected at longer pulse length while maintaining range resolution which can suppress noise (Khodabandeloo et al. 2024), although there are tradeoffs that include larger blind zones near strong boundaries such as the seafloor (Lavery et al. 2017). Additionally, in cases where noise is disproportionately high within specific portions of the signal bandwidth, high-noise bands can likely be identified from the frequency response and filtered to improve SNR.

Avoiding crosstalk while maximizing the available bandwidth can be difficult when using broadband signals transmitted simultaneously (Khodabandeloo et al. 2021, 2024). Given the objective of this study was to compare echo integration between narrowband and broadband signals within a channel, broadband data were collected sequentially across broadband channels to eliminate the potential confounding influence of crosstalk. In practice, eliminating crosstalk via sequential pinging adds a limitation on ping rate for multi-channel data collection. Simultaneous pinging is more practical for surveys and greatly increases the efficacy of other applications that depend on high temporal coverage (e.g. target tracking).

The impact of crosstalk and how it might inform the use of broadband systems for specific applications are discussed in Khodabandeloo et al. (2021) and Khodabandeloo et al. (2024). Though unavoidable, thoughtful processing windows can minimize the impact on processed data while signal properties, especially the transmitted bandwidth, power, and pulse duration, can be modified to reduce crosstalk (Khodabandeloo et al. 2021, 2024). The effects of crosstalk will be more significant for applications involving individual scatterers (i.e. target strength), when the crosstalk can introduce artifacts that impact the frequency response, particularly for weaker targets which can be distorted or masked (Khodabandeloo et al. 2024). For echo integration the impacts of simultaneous pinging can be relatively minor (Khodabandeloo et al. 2021). While this continues to be an ongoing area of study, with appropriate configuration of the transmit signals to reduce crosstalk, the results presented here should apply to simultaneously collected multi-channel data.

With these results in mind, we believe that more widespread use of the capabilities of broadband echosounders in survey applications is worthy of consideration. Given that narrowband-broadband equivalence has been established, this is no longer an impediment to the adoption of broadband techniques when echo integrating. Thus, whether to adopt them represents a balance of what can be gained from broadband sampling versus the additional complexity, data density and computational cost of working with FM signals. With improved processing protocols, decreases in the costs of data storage and improvements to computational capabilities, the potential improvement in classification capability justifies the transition to broadband data collection. Thus, we advocate for the broader adoption of broadband operations and are seeking to transition our efforts to better exploit broadband signals in abundance surveys.

Conclusion

Echo integration of broadband samples, when calculated by averaging the frequency-dependent volume backscatter produced by frequency domain processing, results in echo integrals that are equivalent to narrowband integration of the same nominal frequencies. This use of $S_V(f)$ for integration further streamlines processing methodology by essentially producing echo integration as a byproduct of the calculation of scattering spectra used for echo classification. However, additional hurdles to continued adoption of broadband data for routine abundance surveys remain. Data processing methods

Downloaded from https://academic.oup.com/icesjms/article/82/9/fsaf160/8262704 by National Marine Mammal Lab user on 26 September 2025

are not as well characterized and available in processing software, and data storage and processing requirements relative to narrowband collection can be prohibitive, at least in the near term. In addition, many of the decisions for data collection and processing have not been standardized. Regardless of these needs, the results here show that when there is an expected benefit of collecting broadband data (e.g. vertical resolution for fish tracking, spectra for echo classification), the collection of broadband data does not prohibit making abundance estimates that are consistent with those from traditional narrowband echosounders.

Acknowledgements

The authors would like to thank Lars Nonboe Andersen for motivating them to pursue the averaging of volume backscatter spectra for echo integration. Rick Towler's work on the pyEcholab library made this work possible. We also thank Rolf Korneliussen and Scott Loranger for early discussions that guided the work. We thank Patrick Ressler, Josiah Renfree, and Sandra Parker-Stetter for their comments on the early draft of this work, and the editors and anonymous reviewers for their suggestions which improved this manuscript. Finally, we thank the captain, crew, and science parties of the NOAA ship *Oscar Dyson* for participating in data collection. Any use of trade, firm, or product names is for descriptive purposes only and does not imply endorsement by the US Government. The findings of this paper do not necessarily represent the views of the National Oceanic and Atmospheric Administration.

Author contributions

A.D.R. and C.B. conceived of the project. A.D.R. and C.B. managed the funding acquisition and project administration. A.D.R. and C.B. planned the data collection, and A.D.R. conducted the fieldwork. R.M.L., A.D.R., and C.B. contributed to the methodology, and R.M.L. led the data analysis. R.M.L. led the writing of the original draft, and all authors contributed to review and editing.

Supplementary data

Supplementary data is available at *ICES Journal of Marine Science* online.

Conflict of interest: None declared.

Funding

This publication is partially funded by the Cooperative Institute for Climate, Ocean, & Ecosystem Studies (CICOES) under NOAA Cooperative Agreement NA20OAR4320271, Contribution No. 2025–1463.

Data availability

All echosounder data, including calibration information, are available via the Water Column Sonar Data archive at the NOAA National Centers for Environmental Information at the following DOIs: https://doi.org/10.25921/katszp67, https://doi.org/10.25921/j9aq-t085. The pyEcholab library used to process narrowband and broadband acoustic data is available at https://github.com/noaa-afsc-mace/pyEcholab.

References

Andersen LN, Chu D, Handegard NO *et al.* Quantitative processing of broadband data as implemented in a scientific split-beam echosounder. *Methods Ecol Evol* 2024;**15**:317–28. https://doi.org/10.1111/2041-210X.14261

Bassett C, De Robertis A, Wilson CD. Broadband echosounder measurements of the frequency response of fishes and euphausiids in the Gulf of Alaska. *ICES J Mar Sci* 2018;**75**:1131–42. https://doi.org/10.1093/icesjms/fsx204

Bassett C, Lavery AC, Petitt R *et al.* Autonomous platforms for measuring broadband backscatter. *Proc Mtg Acoust* 2022;**45**:005002. https://doi.org/10.1121/2.0001654

Bassett C, Lavery AC, Ralston D *et al.* Acoustic backscattering at a tidal intrusion front. *Prog Oceanogr* 2023;**219**:103167. https://doi.org/10.1016/j.pocean.2023.103167

Benoit-Bird KJ, Waluk CM. Exploring the promise of broadband fisheries echosounders for species discrimination with quantitative assessment of data processing effects. *J Acoust Soc Am* 2020;**147**:411. https://doi.org/10.1121/10.0000594

Blanluet A, Doray M, Berger L *et al.* Characterization of sound scattering layers in the Bay of Biscay using broadband acoustics, nets and video. *PLoS One* 2019;**14**:e0223618. https://doi.org/10.1371/journal.pone.0223618

Bodholt H. The effect of water temperature and salinity on echosounder measurements. In *ICES Symposium on Acoustics in Fisheries*. Montpellier, 2002. Presentation No. 123.7pp.

Chen C-T, Millero FJ. Speed of sound in seawater at high pressures. *J Acoust Soc Am* 1977;**62**:1129–35. https://doi.org/10.1121/1.381646

Chu D, Stanton TK. Application of pulse compression techniques to broadband acoustic scattering by live individual zooplankton. *J Acoust Soc Am* 1998;**104**:39–55. https://doi.org/10.1121/1.424056

Cotter E, Bassett C, Lavery A. Classification of broadband target spectra in the mesopelagic using physics-informed machine learning. *J Acoust Soc Am* 2021;**149**:3889. https://doi.org/10.1121/10.0005114

De Robertis A, Bassett C, Andersen LN *et al.* Amplifier linearity accounts for discrepancies in echo-integration measurements from two widely used echosounders. *ICES J Mar Sci* 2019;**76**:1882–92. https://doi.org/10.1093/icesjms/fsz040

De Robertis A, Higginbottom I. A post-processing technique to estimate the signal-to-noise ratio and remove echosounder background noise. *ICES J Mar Sci* 2007;**64**:1282–91. https://doi.org/10.1093/icesjms/fsm112

De Robertis A, Jech JM, McKelvey DR *et al.* Development and application of an empirical multifrequency method for backscatter classification. *Can J Fish AquatSci* 2010;**67**:1459–74. https://doi.org/10.1139/F10-075

De Robertis A, Levine M, Lauffenburger N *et al.* Uncrewed surface vehicle (USV) survey of walleye pollock, Gadus chalcogrammus, in response to the cancellation of ship-based surveys. *ICES J Mar Sci* 2021;**78**:2797–808. https://doi.org/10.1093/icesjms/fsab155

Demer DA, Andersen LN, Bassett C *et al.* 2016 USA–Norway EK80 Workshop Report: evaluation of a wideband echosounder for fisheries and marine ecosystem science. ICES Cooperative Research. Report No. 336, 2017, p. 69.

Demer DA, Berger L, Bernasconi M *et al.* Calibration of acoustic instruments. ICES Cooperative Research. Report No. 326, 2015, p. 133.

Ehrenberg JE, Torkelson TC. FM slide (chirp) signals: a technique for significantly improving the signal-to-noise performance in hydroacoustic assessment systems. *Fish Res* 2000;**47**:193–9. https://doi.org/10.1016/S0165-7836(00)00169-7

Downloaded from https://academic.oup.com/icesjms/article/82/9/fsaf160/8262704 by National Marine Mammal Lab user on 26 September 2025

Francois RE, Garrison GR. Sound absorption based on ocean measurements. Part I: pure water and magnesium sulfate contributions. *J Acoust Soc Am* 1982a;**72**:896–907. https://doi.org/10.1121/1.388170

Francois RE, Garrison GR. Sound absorption based on ocean measurements. Part II: boric acid contribution and equation for total absorption. *J Acoust Soc Am* 1982b;**72**:1879–90. https://doi.org/10.1121/1.388673

Grassian B, Roman C, Warren JD *et al.* High-resolution measurements of the epipelagic and mesopelagic ocean by a profiling vehicle equipped with environmental sensors and a broadband echosounder. *Limnol Oceanogr: Meth* 2023;**21**:106–25.

Hazen EL, Horne JK. Comparing the modelled and measured target-strength variability of walleye pollock, *Theragra chalcogramma*. *ICES J Mar Sci* 2004;**61**:363–77. https://doi.org/10.1016/j.icesjms.2004.01.005

Jech JM, Lawson GL, Lavery AC. Wideband (15–260 kHz) acoustic volume backscattering spectra of Northern krill (*Meganyctiphanes norvegica*) and butterfish (*Peprilus triacanthus*). *ICES J Mar Sci*, 2017;**74**:2249–2261. https://doi.org/10.1093/icesjms/fsx050

Jech JM, Foote KG, Chu D *et al.* Comparing two 38-kHz scientific echosounders. *ICES J Mar Sci* 2005;**62**:1168–79. https://doi.org/10.1016/j.icesjms.2005.02.014

Khodabandeloo B, Ona E, Macaulay GJ *et al.* Nonlinear crosstalk in broadband multi-channel echosounders. *J Acoust Soc Am* 2021;**149**:87. https://doi.org/10.1121/10.0002943

Khodabandeloo B, Pedersen G, Forland TN *et al.* Pulse duration, frequency band, and sweep direction effects on crosstalk in wideband backscattering measurements. *J Acoust Soc Am* 2024;**156**:391–404. https://doi.org/10.1121/10.0027912

Korneliussen RJ, Ona E. Synthetic echograms generated from the relative frequency response. *ICES J Mar Sci* 2003;**60**:636–40. https://doi.org/10.1016/S1054-3139(03)00035-3

Kubilius R, Bergès B, Macaulay GJ. Remote acoustic sizing of tethered fish using broadband acoustics. *Fish Res* 2023;**260**:106585. https://doi.org/10.1016/j.fishres.2022.106585

Lavery AC, Bassett C, Lawson GL *et al.* Exploiting signal processing approaches for broadband echosounders. *ICES J Mar Sci* 2017;**74**:2262–75. https://doi.org/10.1093/icesjms/fsx155

Lavery AC, Chu DZ, Moum JN. Measurements of acoustic scattering from zooplankton and oceanic microstructure using a broadband echosounder. *ICES J Mar Sci* 2010;**67**:379–94. https://doi.org/10.1093/icesjms/fsp242

Lavery AC, Wiebe PH, Stanton TK *et al.* Determining dominant scatterers of sound in mixed zooplankton populations. *J Acoust Soc Am* 2007;**122**:3304–26. https://doi.org/10.1121/1.2793613

Levine M, Jones DR. Results of the acoustic-trawl survey of walleye pollock (*Gadus chalcogrammus*) in the Shumagin Islands, Shelikof Strait, and Chirikof shelfbreak, February and March 2024 (DY2024-01 and DY2024-03). AFSC Processed Rep. 2025-07, 2025, p. 82.

Levine RM, De Robertis A, Bassett C *et al.*. Acoustic observations of walleye pollock (*Gadus chalcogrammus*) migration across the US-Russia boundary in the northwest Bering Sea. *ICES J Mar Sci* 2024;**81**:1111–25. https://doi.org/10.1093/icesjms/fsae071

Liu J, Saygili B, Iwasa A *et al.* Effects of fast fourier transform window size on the target strength spectra of tungsten carbide spheres. *Fish Sci* 2023;**89**:147–57. https://doi.org/10.1007/s12562-022-01653-7

Lloyd S. Least squares quantization in PCM. *IEEE Trans Inf Theory* 1982;**28**:129–37. https://doi.org/10.1109/TIT.1982.1056489

Loranger S, Jech MJ, Lavery AC. Broadband acoustic quantification of mixed biological aggregations at the New England shelf break. *J Acoust Soc Am* 2022;**152**:2319. https://doi.org/10.1121/10.0014910

Macaulay GJ, Scoulding B, Ona E *et al.* Comparisons of echo-integration performance from two multiplexed echosounders. *ICES J Mar Sci* 2018;**75**:2276–85. https://doi.org/10.1093/icesjms/fsy111

MacLennan DN, Fernandes PG, Dalen J. A consistent approach to definitions and symbols in fisheries acoustics. *ICES J Mar Sci* 2002;**59**:365–9. https://doi.org/10.1006/jmsc.2001.1158

Mitson RB. Underwater noise of research vessels: review and recommendations. ICES Cooperative Research Report No. 209, 1995, p. 66.

Ona E, Barange M. Single-target recognition, methodology for target strength measurements (with special reference to in situ techniques for fish and micronecton). ICES Cooperative Research. Report No. 235, 1999, p. 28–36.

Ona E, Zhang G, Pedersen G *et al.* In situ calibration of observatory broadband echosounders. *ICES J Mar Sci* 2020;**77**:2954–9. https://doi.org/10.1093/icesjms/fsaa177

Pedersen G, Johnsen E, Khodabandeloo B *et al.* Broadband backscattering by Atlantic herring (*Clupea harengus* L.) differs when measured from a research vessel vs. a silent uncrewed surface vehicle. *ICES J Mar Sci* 2024;**81**:1362–70. https://doi.org/10.1093/icesjms/fsae048

Renfree JS, Andersen LN, Macaulay G *et al.* Effects of sphere suspension on echosounder calibrations. *ICES J Mar Sci* 2020;**77**:2945–53. https://doi.org/10.1093/icesjms/fsaa171

Renfree JS, Demer DA. Optimizing transmit interval and logging range while avoiding aliased seabed echoes. *ICES J Mar Sci* 2016;**73**:1955–64. https://doi.org/10.1093/icesjms/fsw055

Rudin W. *Real and Complex Analysis*. New York: McGraw-Hill, 1987.

Simmonds EJ, Maclennan D. *Fisheries Acoustics Theory and Practice*. 2nd edn. Oxford: Blackwell Science, 2005, 437. https://doi.org/10.1002/9780470995303

Simrad. Simrad EK80 wide band scientific echo sounder Reference manual. 21.15, 2022, 934. https://www.simrad.online/ek80/ref_en/ (23 February 2022, date last accessed).

Stanton TK, Chu D. Calibration of broadband active acoustic systems using a single standard spherical target. *J Acoust Soc Am* 2008;**124**:128–36. https://doi.org/10.1121/1.2917387

Stanton TK, Sellers CJ, Jech JM. Resonance classification of mixed assemblages of fish with swimbladders using a modified commercial broadband acoustic echosounder at 1–6 kHz. *Can J Fish AquatSci* 2012;**69**:854–68. https://doi.org/10.1139/f2012-013

Turin GL. An introduction to matched filters. *IEEE Trans Inf Theory* 1960;**6**:311–29. https://doi.org/10.1109/TIT.1960.1057571

Tušer M, Brabec M, Balk H *et al.* Feasibility of time-dependent amplitude in pulse-compressed broadband acoustic signals for determining the dorsal orientation of fish. *Water* 2023;**15**:1596. https://doi.org/10.3390/w15081596

Urmy SS, De Robertis A, Bassett C. A bayesian inverse approach to identify and quantify organisms from fisheries acoustic data. *ICES J Mar Sci* 2024;**81**:1461–77. https://doi.org/10.1093/icesjms/fsad102

Wall CC, Towler R, Anderson C *et al.* PyEcholab: an open-source, Python-based toolkit to analyze water-column echosounder data. *J Acoust Soc Am* 2018;**144**:1778. https://doi.org/10.1121/1.5067860

Handling editor: Olav Rune Godø

Published by Oxford University Press on behalf of International Council for the Exploration of the Sea 2025. This work is written by (a) US Government employee(s) and is in the public domain in the US.

Downloaded from https://academic.oup.com/icesjms/article/82/9/fsaf160/8262704 by National Marine Mammal Lab user on 26 September 2025